SCIENCE CHINA
Technological Sciences

September 2012 Vol.55 No.9: 2453–2461
doi: 10.1007/s11431-012-4935-1

Computational methods and engineering applications of static/dynamic aeroelasticity based on CFD/CSD coupling solution

YANG GuoWei*, ZHENG GuanNan & LI GuiBo

LHO of Institute of Mechanics, Chinese Academy of Sciences, Beijing 100190, China

Received February 18, 2012; accepted April 28, 2012; published online July 15, 2012

The CFD/CSD coupling method is turning into the main research direction for the static/dynamic aeroelastic analyses. If one wants to use the method for the complex engineering aeroelastic problems, he needs to investigate the relative aeroelastic algorithms, such as the numerical computational method of unsteady aerodynamic forces, equivalent low-dimensional structural finite element model and the solution method of structural dynamic equations, data transfer technique between fluid and structure, the moving grid method, etc. Besides, he also needs to improve the computational efficiency by such as massive parallel CFD algorithm, reduced-order model (ROM) of unsteady aerodynamic forces, etc. In this paper, based on the authors' recent investigations, the research progresses in computational aeroelastic methods and their applications to engineering problem are summarized.

aeroelasticity, CFD/CSD, ROM, active flutter suppression

Citation: Yang G W, Zheng G N, Li G B. Computational methods and engineering applications of static/dynamic aeroelasticity based on CFD/CSD coupling solution. Sci China Tech Sci, 2012, 55: 2453–2461, doi: 10.1007/s11431-012-4935-1

1 Introduction

Along with the progress of CFD techniques, in the 90's of last century, the CFD/CSD coupling method began to be used for investigation of aeroelastic problems [1–3]. For the calculation of unsteady aerodynamic forces, Euler equations based on unstructured grid and Euler or Navier-Stokes equations based on multi-block structured grids were mainly used. For the calculations of structural deformation, the generalized structural equations of motion based of linear structural modes were adopted. For the coupling method between fluid and structure, the loosely method was mainly used and the computational time accuracy was only first-order. For data transfer between fluid and structure, the two-dimensional surface interpolation method from linear aeroelastic analyses was mainly adopted and only the single-directional structural deformation was considered. For the adaptive dynamic grid techniques, the grid regeneration or trans-finite interpolation (TFI) was used to get the new CFD grid for the structured grid of simple configurations, and the linear-spring method or additional twist-spring network for unstructured grid. For the geometrical models, only simple configurations such as two-dimensional airfoils, sole wings, etc. were considered.

As the extensive investigations of computational aeroelastic methods, Gordiner et al. [4] put forward an implicit tightly coupling CFD/CSD method to improve computational time accuracy. Wendland et al. [5] developed a three-dimensional data interpolation method between fluid and structure based on radial basis function (RBF). Clarence [6] deduced a three-dimensional formation with linear and twist spring networks based on linear spring model of Batina [7] and two-dimensional twist spring model of Fahart [8]. These research achievements indicate that the

*Corresponding author (email: gwyang@imech.ac.cn)

static/dynamic aeroelastic simulation methods are becoming mature.

For the CFD/CSD coupling method to treat complex static/dynamic aeroelastic engineering problems, there are still some technical challenges. The first is the unsteady flow solver for extra complex configurations. Single- and multi-block structured grids are hard to be generated and unstructured grid cannot simulate the viscous flow due to grid isotropy. In order to satisfy the requirement of viscous flow simulation, anisotropic grid cells need to be generated in boundary layer and unsteady flow solver based on hybrid grid needs to be developed. The second is the lower computational efficiency with the CFD/CSD coupling method which is mainly limited by the flow calculation. The massive partition parallel algorithm for the hybrid grid-based CFD solver is necessary, which is confronted with the technical hindrances of load balance and data communication. The third is how to extend the traditional spring network method to dynamic grid deformation of hybrid grid and have a higher deformation efficiency. Only these hindrances are settled one by one, aeroelastic analysis tool for aeronautical and astronautical engineering problem can be established.

To further improve aeroelastic computational efficiency and extend the CFD-based aeroelastic analysis method to the applications of multidisciplinary optimization design, servo-aeroelastic analysis, flutter active suppression, and the gust alleviation, etc., reduced order models (ROMs) of unsteady aerodynamic forces need to be developed to construct state-space analytical models. At present, the ROMs of Arma [9], Volterra [10], Pod [11], Anns [12] and so on are being investigated extensively. These ROMs are mainly validated with two-dimensional airfoils and three-dimensional simple wing shape. It is believed that ROMs can be used for aeroelastic integrated design for complex engineering problem.

In the paper, our recent progresses on the analysis methods and partial engineering applications in static/dynamic aeroealstic investigation are emphatically depicted.

2 CFD/CSD coupling computational method

2.1 Hybrid grid-based parallel fluid solver

For complex engineering configurations, hybrid grids can be generated with ICEM or Gridgen software, which contain the four cell types of tetrahedron，hexahedron，prism and pyramid. To guarantee the simulation of viscous boundary layers, in the inner region of near surfaces, anisotropic grid cells of prim or hexahedron are utilized. In the outer region, tetrahedron grid cells are generated and with pyramid grid cells for the transition between the two regions.

By adopting cell-vertex finite volume discretization, the fluid solver is developed based on unsteady Reynolds averaging Navier-Stokes equations and two-equation eddy viscosity turbulence models. The control volume consists of grid line center, grid surface center and grid volume center of adjacent cells. The convective terms of fluid equations are dicretized by a series typical second-order schemes such as Roe [13], Hllew [14], Ausm [15], Hllc [16], etc. and the limiter of Venkatakrishnans [17] is adopted to reconstruct the left and right primitive flow variables. In these schemes, comparatively speaking, the HLLEW scheme possesses more robustness and lower diffusion. The viscous terms are discreted by the second-order center difference scheme and k-ω and k-ω SST two-equation turbulence models are employed in the solver [18, 19]. To save computational time, it is suggested to use this model for the turbulence simulation due to no distance function used in k-ω model.

Implicit time-marching scheme without the limitation of stability condition is the main method to improve computational efficiency. For the serial fluid solver, the implicit LU-SGS scheme of Sharov et al. [20] is used by unstructured grid reconstruction. For the difficulty of parallel treatment with LU-SGS scheme which needs to transfer the additional inner boundary variables，the LU-DPR scheme of Michael et al. [21] which is suitable of partition parallel computation of unstructured grid is adopted. For these two implicit time-marching methods, the diagonal-dominated matrix decomposition and the inner iteration method of Jameson [22] are adopted to improve computational efficiency and time accuracy. Theoretically, the second-order real time accuracy can be attained when the inner iterations tend to infinity. In the same way, the generalized structural equations are also discretized with the inner iteration scheme. In the calculation process, for each real time step, the fluid and structural solvers are iterated synchronously for a steady solution. The time accuracy of the coupling solution can achieve second-order. However, in practical calculation, we usually take the number of inner iteration steps as 20.

Partition parallel strategy is adopted for the solution of unsteady CFD solver. The traditional multi-series K-way method of Pmetis [23] is used for grid partition, which can approximately guarantee the load balance and less inner boundary nodes. A new MPI communication way of layered coloration developed by the authors [24] is used, which can decrease the communication stems and improve communication efficiency. By validation, the parallel computational efficiency can achieve above 90%.

2.2 Structural deformation solver

It is very burdensome and complex for vehicles to construct the static finite element models in detail, which have several millions of structural freedoms. For the structural dynamic analysis, it is necessary to simplify the finite element model to several hundreds of freedoms based on the stiffness equivalent principle to match the important structural fre-

quencies, structural modes and mass distributions with its real structure. At present, the Nastran software is mainly employed to construct the structural finite element model. For static/dynamic aeroelastic calculations, the structural flexibility matrix and generalized mass, structural modes and natural frequencies are outputted respectively. Due to the three-dimensional surface interpolation between fluid and structure used, it is necessary that the distribution of surface structural points can reconstruct the real vehicle shape, whose number is less than 1000 in general. In the paper, three-dimensional structural deformation is considered, the structural flexible matrixes and modes in the three coordinate directions need to be given. If only the main directional deformation is considered, the structural data in the other two directions can be taken as zero.

For the static aeroelastic calculation, structural static balance equations are solved. For the flutter calculation, in general, the generalized structural equations of motion are solved. Under the assumption of linear structure, the structural modes and their frequencies are unchangeable in the structural deformation processes, and the generalized aerodynamic forces are obtained by the unsteady CFD calculation instantaneously. Similar to CFD time discretization, the inner iteration scheme is also used to improve the time accuracy of CSD [25]. As the number of inner iteration tends to infinite, the time accuracy can be arrived at second-order.

2.3 CFD/CSD coupling method

Because both of fluid and structural equations are discretized with inner iteration schemes, to improve the coupling time accuracy, CFD and CSD are iterated at each real time step, so-called tightly coupling method, the coupling time accuracy can attain the second-order.

Due to the independent model constructions of CFD and CSD, the surface grids between fluid and structure cannot correspond to each other on the surface; in general, the structural surface nodes are one-order less than the fluid nodes. We need to transfer the CFD loads to structural surface nodes and the structural deformation determined to CFD surface nodes. For flutter calculations, based on three-dimensional RBF interpolation [5], the structural modes can be pre-interpolated to CFD surface grid nodes in advance to improve computational efficiency. However, for the static aeroelastic calculation, it is necessary to interpolate the structural deformation to CFD surface nodes with RBF instantly and obtain the aerodynamic loads on the structural nodes by the transfer matrix based on the virtual work principle.

After the CFD surface node deformations are known, it needs the CFD volume grids to move with the structural deformation, namely the dynamic grid technique. For the structured grid deformation, TFI interpolation [26] is usually used. For unstructured grid deformation, the spring network method is usually used. For hybrid grid deformation, there is still no any direct dynamic grid deformation method. By combining the spring network method [6] with the algebraic interpolation method [27], a new dynamic deformation method for hybrid grid was developed by the authors [28]. It contains two steps. The first is to generate a coarser unstructured background grid in both fluid and solid regions for the dynamic deformation with the traditional spring network method. Since the number of background grid cells is one-order less than that of CFD grid, its grid deformation efficiency can be improved largely. The second is to interpolate the deformation of each CFD grid node one by one with the background grid cell containing the CFD grid node by volume weighted average. Since the relation between CFD grid and background grid can be predetermined and the time consuming of the above algebraic interpolation can be ignored, the new developed method has a higher deformation efficiency and is suitable to the grid deformation of any topological CFD grid. The background grid is generated in the solid region, which can guarantee any CFD node to locate in the interior of one inner background grid cell to avoid extrapolation.

3 ROMs of unsteady aerodynamic forces

Much computational time is still needed for the direct CFD/CSD coupling calculation even both the massive parallel algorithm and implicit time discretization method are adopted. The large part of computational time is consumed in the CFD calculations, which limits the engineering application of fast aeroelastic evaluations and time-domain servo-aeroelastic analysis and integrated aeroelastic optimization. To solve these problems, ROMs were put forward for the replacement of real time calculation of unsteady aerodynamic forces. At present, ROMs are divided mainly into two kinds. The first is to consider the CFD/CSD model as a system and ROMs are constructed based on systemic identification by the input-output characteristics of excitations and responses, whose typical models are ARMA [9] and Volterra series models [10]. The second is to reduce the order of fluid discretization matrix by characteristic analysis to obtain the main flow modes, whose typical model is POD-based ROM [11]. All of these ROMs are established based on the assumptions of static flow nonlinearity and dynamic flow linearity.

3.1 ROMs based on systemic identification

For the ARMA ROM, the generalized aerodynamic forces of the kth time step are expressed with the linear function of previous na input values and nb output values. In general, the typical 3211 signal having a broad frequency range is taken as the input excitation signal for the unsteady CFD model and generalized aerodynamic forces as output. The best fitness approximations for the coefficients of na, nb and

constant coefficient matrix are evaluated by the least-square method. The established ARMA ROM model can be replaced by the unsteady CFD calculation for the flutter and servo-aeroelastic calculation.

Volterra model is a functional series, which can approach with any accuracy to a nonlinear time-invariant system. In general, the step function is taken as the input signal for the second Volterra discretization function, by deducing and neglecting the second-order terms, the Volterra ROM can be obtained.

The determined ROMs and the generalized structural equations of motion are first expressed with the discretized state-space forms. Then the aeroelastic state-space model is obtained by the combination of these two models. The flutter dynamic pressure and frequencies can be determined by the root locus of the characteristic matrix or direct time-marching method. Since less time is for the solution of aeroelastic state-space model and only several hundreds of CFD calculations are needed for each input signal of structural modes, ROM can improve the computational efficiency by about two orders, as compared with the direct CFD/CSD coupling solution. It is more important that the ROM models are easy to couple the control system to get the areoelastic closed-loop control model, therefore the flutter active suppression and servo-aeroelasticity can be investigated.

Relatively, ARMA is sensitive to the input signal. To guarantee the excitation of requisite frequency ranges, it needs to adjust the time interval of input signal again and again for the model training. However, the Volterra series model is insensitive to the input signal and is more suitable to engineering applications.

3.2 ROM based on POD

The construction of POD-based ROM contains two steps. The first is to linearize the fluid equations and structural equations of motion at the static balance position. The second is to get POD basis and kern functions, and further to obtain the orthogonal sub-space by the calculation of characteristic vector. The POD ROM can be deduced by the projection of whole flow-field into the sub-space. In general, the triangle pulse signal is used as input signal to excite the linearized fluid governing equations to get snapshot matrix. It is difficult and expensive to calculate quickly and exactly the Jacobian matrixes of the linearized fluid governing equations. To improve the computational accuracy, the automatic differential method of adjoint derivative solutions [29] has been utilized successively.

Compared with the systemic identification models, the POD model has a higher accuracy, however, lower efficiency and larger memory requirement. At present, only two dimensional airfoils and Euler equations have been investigated, and it is still hard to solve aeroelastic engineering problem.

4 Application examples

4.1 Flutter of vertical tail with control surface

The model of vertical tail with control surface is shown in Figure 1. The first four structural modes as shown in Figure 2 are taken for the flutter calculation, in which the first and third are the dominated modes of stabilizer and the second and fourth are the dominated modes of the control surface. Mach number is taken as 0.15–1.1, for each Mach number, flutter boundaries are searched by the changes of dynamic pressures, namely, for two given dynamic pressures, the generalized structural displacements present small divergence and convergence, respectively, then the flutter boundary can be interpolated and validated.

Figure 3 gives the curves of the flutter speed and frequency vs. Mach number. For Mach numbers less than 0.9 and large than 1, the classical bending/twisting flutter phenomenon appears. However, for Mach numbers between 0.9 and 1, it behaves an abnormal change. Unsteady pressure

Figure 1 The model of vertical tail with control surface.

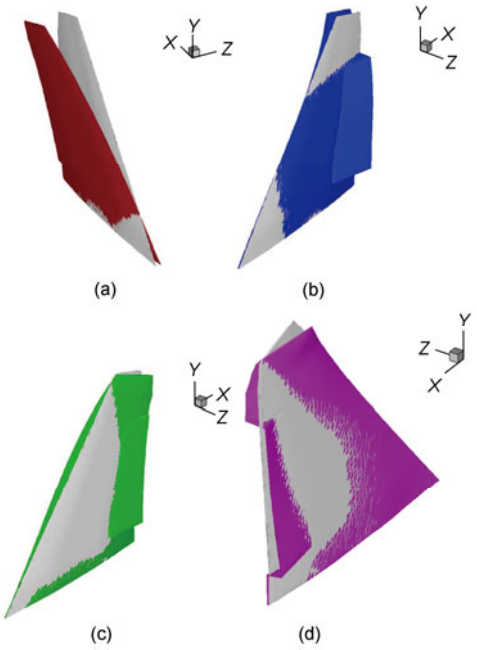

Figure 2 The first four structural modes of vertical model.

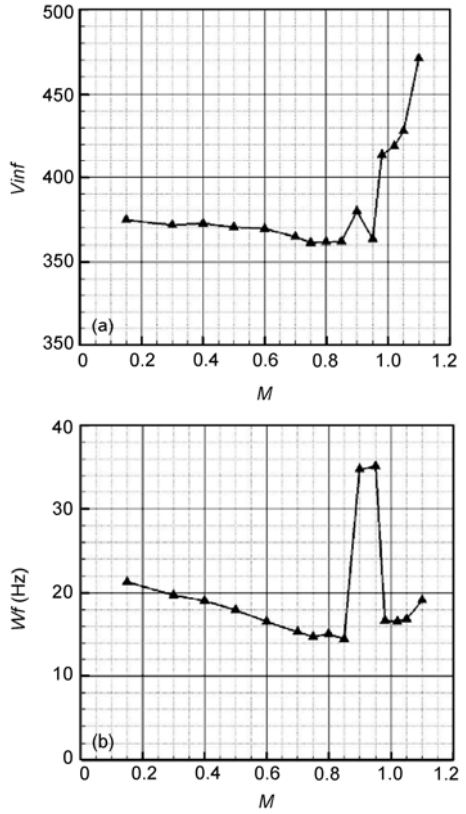

Figure 3 Flutter boundaries of the vertical tail. (a) Flutter speed; (b) flutter frequency.

distributions of different times at 50% spanwise position for the Mach numbers of 0.8 and 0.95 are shown in Figure 4. For the Mach number of 0.8, aerodynamic loads are mainly supplied by the structural deformation of the stabilizer. However, for the Mach number of 0.95, aerodynamic loads are mainly supplied by the control surface deflection similar to the phenomenon of aileron buzz, but its frequency is unequal to that of the control surface mode, which is a coupling flutter characteristic dominated by the control surface modes and partly associated with the second bending mode.

4.2 Flutter of all moving horizontal tail

Figure 5 shows the aircraft model with body, wings, all moving horizontal tails and twin vertical tails. To investigate the flutter of all moving horizontal tails, the body, wings and horizontal tails are assumed to be rigid and only horizontal tails are considered as flexible. Its first four structural modes are taken as the flutter calculations shown in Figure 6. The real line of Figure 7 presents the curve of flutter speed vs. Mach number. The flutter speed has no obvious transonic dip, however, the abnormal changes occur in the Mach numbers of 0.8–1.1. Whether the flow field interaction of adjacent vertical tail or the main wing influences this? The dashed lines in Figures 7(a) and (b) depict the flutter boundaries without vertical tail and without main wing, respectively. It indicates that the abnormal flutter phenomenon is caused by the flow interaction between the main wing and the horizontal tail. The flows are also analyzed with and without the main wing. At the transonic Mach number, we can find that the normal shock appears on the wing surfaces and a subsonic flow region exists ahead of the horizontal tail, which results in the abnormal flutter boundary. It is also indicated that the flutter analysis for aircraft parts needs to consider the interactions of whole flows.

4.3 Jig shape correction with static aeroelastic method

For the cruise aircraft shape, its jig shape can be obtained by unloading its engine trust force, mass force, aerodynamic force and structural elastic force. The structural flexible matrix is obtained by finite element model and its aerodynamic load can be calculated if the rigid cruise shape, the engine trust force and the mass force of aircraft are known. Then the jig shape can be determined by the solution of the static balance equation only with one step calculation. The comparison of cruise (light color) and jig (saturated color) shapes is shown in Figure 8(a). If the jig shape is reasonable, by the assumption of flexible matrix fixed with linear structure, the static aeroleatsic positive calculation can be used

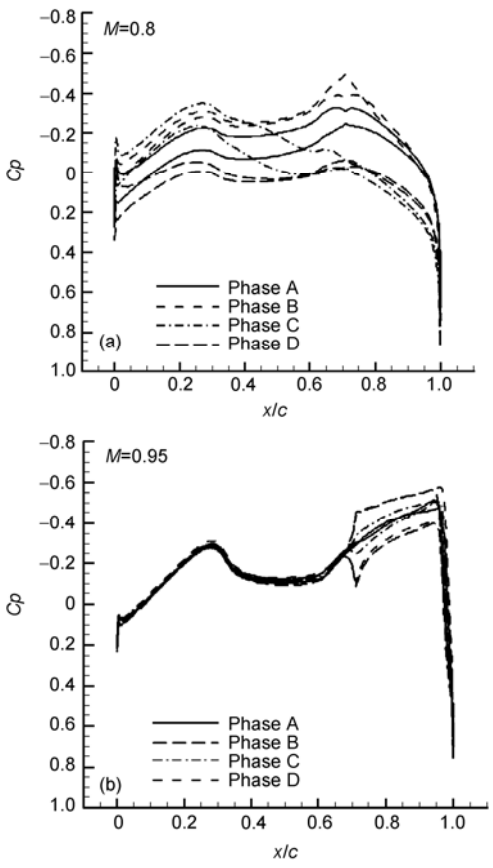

Figure 4 Unsteady pressure distributions at 50% spanwise position. (a) Mach number 0.8; (b) mach number 0.95.

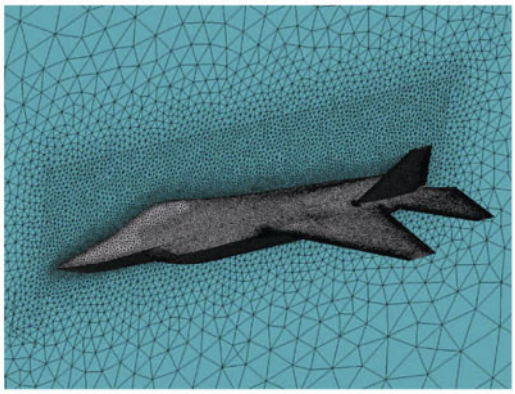

Figure 5 Aircraft model.

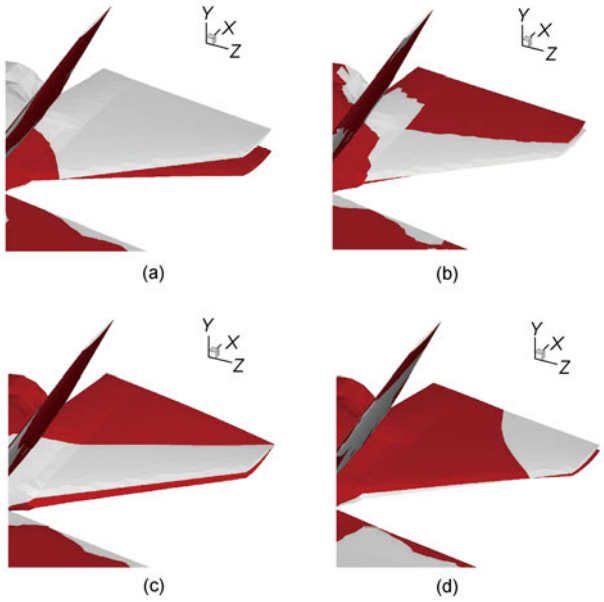

Figure 6 The first four structural modes of all-moving horizontal tail.

for the method of validation of jig shape correction. If its static aerelastic performance and shape can be reverted to those of the cruise shape, then it is available. Table 1 gives the performance comparison between the cruise shape and the static aeroelastic shape, which agree very well with each other. It indicates that the jig shape correction method is reliable.

According to technical requirement, the rectilinear line of wing leading edge is better for product. As we know, the main effect factor for the aerodynamic performance is the spanwise twist distribution. The modified jig shape can be determined again by only modification of twist distribution of wing based on the crusie shape. Figure 8(b) shows the shape comparison between the cruise (light color) and the modified (saturated color) jig shapes. The aerodynamic performance of modified jig shape can be calculated with the static aeroelastic positive analysis. Table 2 gives the comparison between the modified jig shape and the cruise

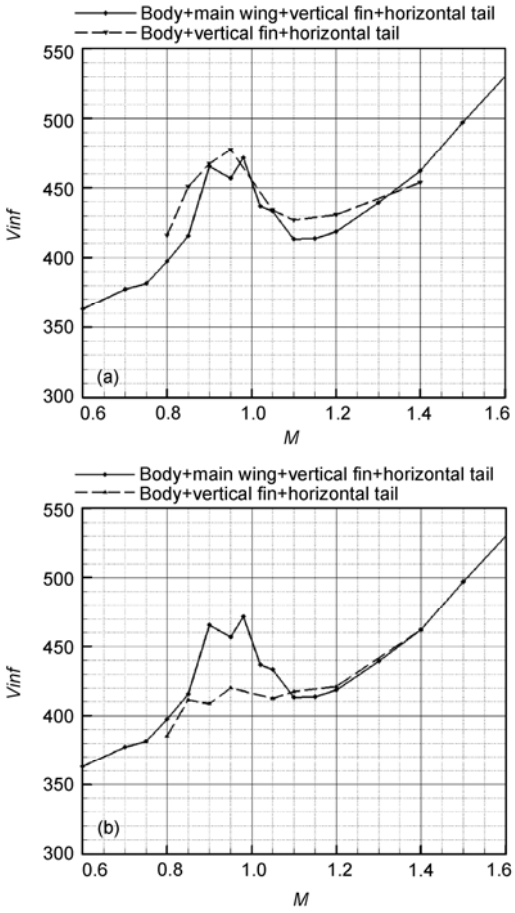

Figure 7 Flutter of horizontal tail effected by vertical tail and main wing. (a) Flutter boundaries with and without the vertical tail; (b) flutter boundaries with and without the main wing.

Table 1 Performance comparison of cruise and jig shapes

	Cruise	Jig	Difference
C_l	0.56514	0.56510	0.0069%
Cd	0.04298	0.04299	0.036%

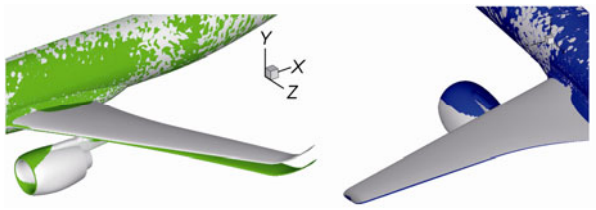

Figure 8 Jig shape correction of cruise shape. (a) Comparison of jig and cruise shapes; (b) comparison of modified jig and cruise shapes.

Table 2 Aerodynamic performance of cruise and modified jig shapes

	Cruise	Modified jig	Difference
C_l	0.56514	0.56226	–0.051%
Cd	0.04298	0.04299	0.023%

shape, whose performance can be nearly recovered. However, the lift coefficient decreases slightly and the drag coefficient increases slightly, which may be induced by the three-dimensional bending effects of the wing. By zooming in and out of the spanwise twist distribution with an equivalent scale，the twist distribution can be modified again based on the equivalence of lift coefficient with the cruise shape. However, it is hard to revert completely to that of cruise design.

4.4 Comparison and application of ROMs

The model of AGARD 445.6 wing has become a standard example for the transonic aeroelastic validation, which is a 45° swept wing, has a root chord length of 21.96 inches and span length of 30 inches. The first four structural frequencies of its weekend model are 9.6, 38.2, 48.3 and 91.5 Hz, which correspond to the modes of the first bending, the first twisting, the second bending and the second twisting. More detail data can be found in ref. [30].

For the fixed test Mach number of 0.96, a comparison for ARMA, Volterra, POD ROMs and CFD/CSD was carried out. It indicates that the ARMA ROM is sensitive to input signal and needs model training again and again, the Volterra ROM is relatively exact and effective and is suitable for engineering problem, and the POD ROM is more exact but of lower efficiency. Figures 9 and 10 give the generalized displacement time histories solved by Volterra and POD ROMs and direct CFD/CSD coupling solution at Mach number of 0.96 and dynamic pressure of 41.6861 b/ft^2. The real lines in Figures 9 and 10 represent the results of Volterra and POD ROMs and the block line is the result of CFD/CSD, which agree well with each other. The accuracy of POD ROM is a little better than that of the Volterra model, however, the efficiency of Volterra ROM is about 10 times of POD ROM.

The Volterra ROM of unsteady aerodynamic force and the generalized structural equations of motion can be written as the state-space models. By further introducing the close-loop control model of additional unsteady aerodynamic force of control surface deflection, the flutter active suppression state-space model can be obtained. In here, since only the flutter suppression method is validated, we assume that the rotating axis of control surface locates at 20% of spanwise position of tailing edge and the structural modes are unchangeable. Adopting LQR and LQG control rules, the flutter can be suppressed. Figure 11 gives the active suppression effect, where LQR is added when the flutter appears at Mach number of 0.834 and dynamic pressure of 109.611 b/ft^2. Figure 12 gives the active suppression effect, where LQG control is added at the beginning of flutter. Relative to the LQR control, the LQG model is more

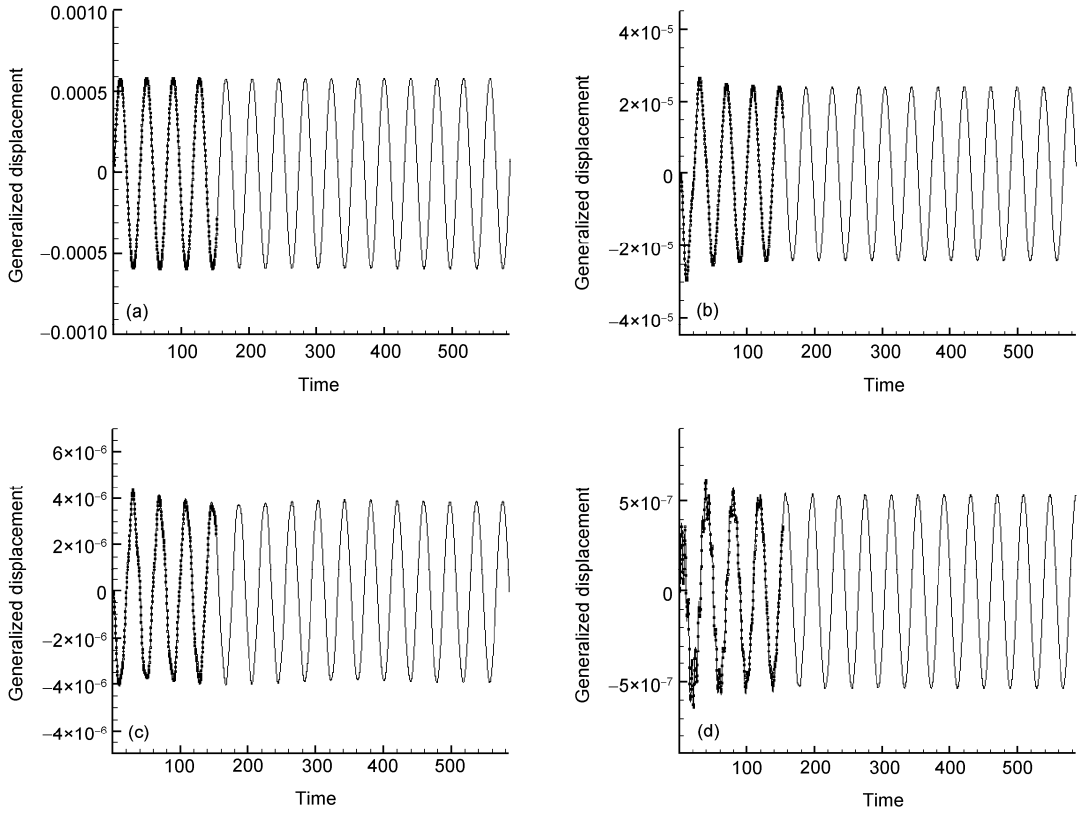

Figure 9 The generalized displacement histories calculated by Volterra ROM and CFD/CSD at Mach number of 0.96 and dynamic pressure of 41.6841 b/ft^2. (a) First-order; (b) second-order; (c) third-order; (d) fourth-order.

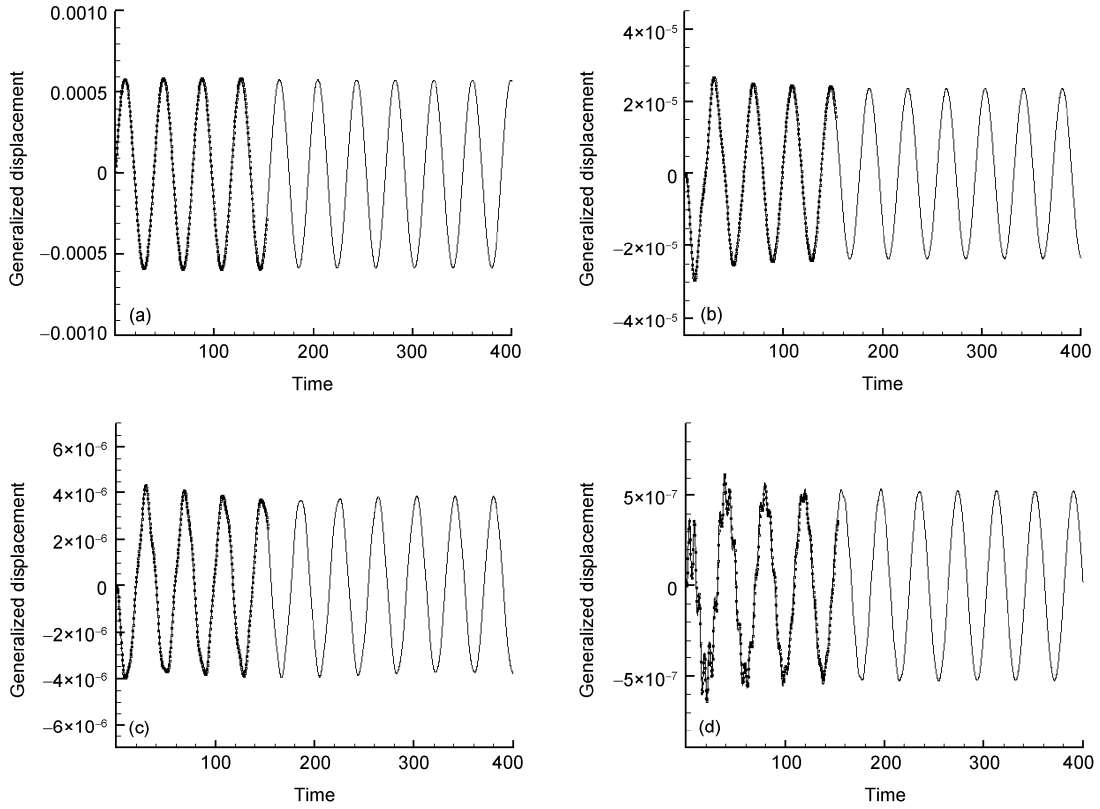

Figure 10 The generalized displacement histories calculated by POD ROM and CFD/CSD at Mach number of 0.96 and dynamic pressure of 41.6841 b/ft^2.

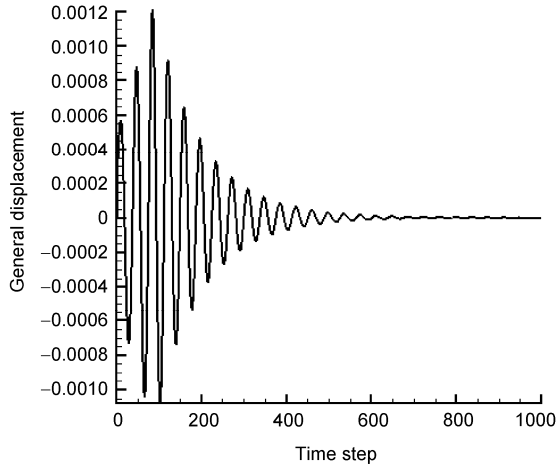

Figure 11 First generalized displacement time history with LQR control at Mach number of 0.834 and dynamic pressure of 109.611 bf/ft^2.

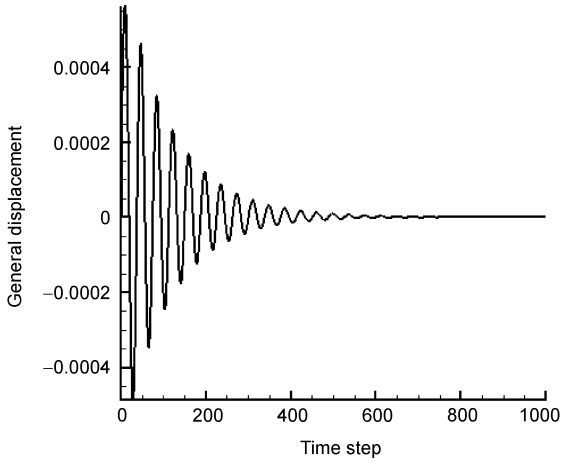

Figure 12 First generalized displacement time history with LQG control at Mach number of 0.834 and dynamic pressure of 109.611 bf/ft^2.

suitable for engineering application because all state variables are given by its state observer.

5 Conclusions

The paper summarized our researches in recent years on the CFD/CSD-based static/dynamic aeroelastic methods and partly engineering applications and ROM investigations. Some new flutter phenomena and mechanisms were analyzed. At last, the accuracies and efficiencies were compared for the three ROMs and the flutter active suppression based on Volterra ROM with LQR, and LQG control rules were also investigated. It is indicated that the flutter active suppression has good application foreground in the future.

The developing tends of aeroelastic investigation will

aim at two aspects. One aspect is, on the basis of the traditional static/dynamic aeroelastic investigations, to extend the aeroelastic investigation ranges, such as the time-domain analysis methods of servo-aeroelasticity, gust alleviation, thermal aeroelasticity, etc. The second is, by developing the aeroelastic integrated optimization technique and applying the primary design phase of aerodynamic/structural selection, to make the aeroelastic analysis an active design tool to improve the whole aircraft performance and design efficiency.

1 Guruswamy G P. Vortical flow computations on swept flexible wings using navier-stokes equations. AIAA J, 1990, 28: 2077–2133
2 Lee-Rausch E M, Batina J T. Wing flutter computations using an aeroelastic model based on the navier-stokes equations. J Aircraft, 1996, 33: 1139–1147
3 Alonso J J, Jameson A. Fully-implicit time-marching aeoelastic solutions. AIAA Paper94-0056, 1994
4 Gordiner R E, Melville R B. Transonic flutter simulations using an implicit aeroelastic solver. J Aircraft, 2000, 37: 872–879
5 Holger W. Computational aspects of radial basis function approximation. Stud Comp Math, 2006, 12: 231–256
6 Clarence O, Burg E. A robust unstructured grid movement strategy using three-dimensional torsional springs. AIAA Paper 2004-2529, 2004
7 Batina J T. Unsteady euler airfoil solutions using unstructured dynamic meshes. AIAA Paper 89-0115, 1989
8 Farhat C, Degand C, Koobus B, et al. Torsional springs for two-dimensional dynamic unstructured fluid meshes. Comp Meth Appl Mech Eng, 1998, 163: 231–245
9 Cowan T J, Andrew S. Accelerating CFD-based aeroelastic predictions using system identification. AIAA paper 1998-4152, 1998
10 Munteanu S, Rajadas J, Nam C, et al. A volterra kernel reduced-order model approach for nonlinear aeroelastic analysis. AIAA 2005-1854, 2005
11 Tang D, Kholodar D, Juang J, et al. System identification and proper orthogonal decomposition method applied to unsteady aerodynamic. AIAA J, 2001, 39: 1569–1576
12 Wang B B, Zhang W W, Ye Z Y. Unsteady nonlinear aerodynamics identification based on neural network model (in Chinese). Acta Aeronautic Et Astronautica Sinca, 2010, 31: 1379–1388
13 Roe P L. Approximate riemann solvers, parameter vectors, and difference schemes. J Comp Phys, 1981, 43: 357–372
14 Obayashi S, Guruswamy G P. Convergence acceleration of an aeroelastic Navier-Stokes solver. AIAA Paper 94-2268, 1994
15 Liou M S. A sequel to AUSM: AUSM+. J Comp Phys, 1996, 129: 364–382
16 Harten A, Lax P D, van Leer B. On upstream differencing and godunov-type schemes for hyperbolic conservation laws. SIAM Review, 1983, 25: 35–61
17 Venkatakrishnan V. On the accuracy of limiters and convergence to steady state solutions. AIAA Paper 93-0880, 1993
18 Menter F R. Two-equation eddy-viscosity turbulence models for engineering applications. AIAA J, 1994, 32: 1598–1605
19 Menter F R. Zonal two equation k-ω turbulence models for aerodynamic flows. AIAA Paper 93-2906, 1993
20 Sharov D, Nakahashi K. Reordering of hybrid unstructured grids for lower-upper symmetric gauss-seidal computations. AIAA J, 1998, 36: 484–486
21 Michael J W, Graham V C, Marco P. Data-parallel lower-upper relaxation method for the navier-stokes equations. AIAA J, 1996, 34: 1371–1377
22 Yoon S, Jameson A. Lower-upper symmetric gauss seidel method for the euler and navier-stokes equations. AIAA J, 1988, 26: 1025–1026
23 Karypis G, Kumar V. Multilevel k-way Hypergraph Partitioning. Technical Report TR 98-036, Department of Computer Science, University of Minnesota, 1998
24 Zheng G N, Deng S C, Han T L, et al. Investigation on parallel implicit computational method based on hybrid grid Navier-Stokes equations (in Chinese). Chin J Appl Mech, 2011, 28: 211–218
25 Yang G W, Obayashi S, Nakamichi J. Aileron buzz simulation using an implicit multiblock aeroelastic solver. J Aircraft, 2003, 40: 580–589
26 Wong A S F, Tsai H M, Cai J, et al. Unsteady flow calculations with multi-block moving mesh algorithm. AIAA-2000-1002, 2000
27 Liu X Q, Qin N, Xia H. Fast dynamic grid deformation based on delaunay graph mapping. J Comp Physics, 2006, 211: 405–423
28 Zheng G N, Yang G W. Hybrid grid deformation method based on background grid (in Chinese). J Vib Eng, 2011, 24: 473–481
29 Giles M B, Ghate D, Duta M. Using automatic differentiation for adjoint cfd code development. In: Indo-French Workshop, 2005
30 Yetes E C Jr. AGARD standard aeroelastic configurations for dynamic response I-wing 445.6. AGARD-R-765, 1998